TOP-LEVEL DESIGNS OF A HYBRID LOW FIELD MRI-CT SYSTEM FOR PULMONARY IMAGING

Venkata R Yelleswarapu[1], Fenglin Liu[2,3], Wenxiang Cong[2], Ge Wang[2],* IEEE Fellow
[1] Biomedical and Electrical Engineering Departments, Boston University, MA 02215 USA
[2] Center for Biotechnology and Interdisciplinary Studies, Rensselaer Polytechnic Institute, NY 01280 USA.
[3] Key Lab of Optoelectronic Technology and System, Chongqing University, Chongqing 400044, China
(*e-mail: wangg6@rpi.edu)

***Abstract*— We previously discussed "omni-tomography", but intrinsic conflicts between the magnetic fields of the MRI and the x-ray tube within the CT are inherent. We propose that by using low-field MRI with a negligible fringe field at the site of the CT source, it is possible to create a CT-MRI system with minimal interference. Low field MRI is particularly useful for lung imaging, where hyperpolarized gas can enhance the signal. Three major designs were considered and simulated, with modifications in coil design and axis allowing for further variation. The first uses Halbach arrays to minimize magnetic fields outside, the second uses solenoids pairs with active shielding, and the third uses a rotating compact MRI-CT. Each system is low field, which may allow the implementation of a standard rotating CT. Both structural and functional information can be acquired simultaneously for a true hybrid image with matching temporal and spatial image acquisition.**

I. INTRODUCTION

MAGNETIC Resonance Imaging (MRI) and X-ray Computed Tomography (CT) are widely used imaging techniques that provide complementary information about patient anatomy. CT methods are primarily used to image hard tissue such as bone while MRI offers high contrast in soft tissue. This high contrast can be used to diagnose unhealthy tissue or detect cancer. MRI is highly sought during lung imaging due to its lack of harmful radiation and superiority in the assessment of functional changes in the pulmonary system such as perfusion [1].

Due to the inherent poor contrast from fluid-air interface in the lung, called the susceptibility artifact, the signal needs to be enhanced with hyperpolarized gas. ^{3}He is 10^5 more polarized than the thermal polarization of water molecules, allowing a lower concentration of the gas to give sufficient details. The addition of CT can further enhance the structural detail, but the interference between the magnetic fields and the xray tube such as electron deflection and rotating anode deceleration [2-5].

Low field MRI has been successfully used to image lung physiology at 10mT[6], and the breakthrough of interior tomography in CT and MRI allows the use of a region of interest within a field of view, allowing for more compact machines to be built with less stringent zones of homogeneity[7-10]. This effect has been studied extensively, with various papers about using robust x-ray tubes, shielding, and placing the X-ray system over 6 ft from the CT scan are described without a true hybrid system in very low field magnetic fields [2-5]. The minimal threshold before significant defocusing for rotating anodes and electron deflection occur at 20mT and 3mT, respectively.

The use of low field MRI is advantageous for reducing the interference between the two systems. With the use of low field MRI, the CT scanner can be directly implemented at the center of the scanner combination, allowing for simultaneous acquisition with spatial and temporal equivalence. Thus, by combining the two systems, it will be possible to acquire a high resolution image of the pulmonary system with quantitative measurements of perfusion, ventilation, gas diffusion, and cancer nodule properties.

II. METHODS

The Lortenz Force (1) describes how the electron beam is affected by a perpendicular magnetic field, while the Biot-Savart Law (2) describes magnetic fields generated by current in a solenoid. Columbian physics dictated the implementation of permanent magnets.

$$(1)\vec{\boldsymbol{F}} = \frac{d\vec{\boldsymbol{p}}}{dt} = -e(\vec{\boldsymbol{E}} + \vec{\boldsymbol{v}}\, x\, \vec{B}) \qquad (2)\vec{\boldsymbol{B}} = \frac{\mu_0}{4\pi}\int_C \frac{Id\vec{l}\, x\, \vec{r}}{|\vec{r}|^3}$$

To visualize the resulting fields, Finite Element Analysis packages QuickField™ and Vizimag were used. Various geometric configurations, B-H curves based on available data of Neodymium (NdFeB) magnets, currents, etc. were modeled to generate possible configurations of a low fringe field MRI with a minimum of 50mT strength at the center.

Based on this system design, we implement the simulation of the stationary CT to verify the quality of image reconstruction on a region of interest in the object with parameters described in our previous work [11]. The phantom was produced by a sheep lung CT slice image with 332×244 pixels. We used fan-beam geometry to simulate the x-ray imaging mode, and 21 equi-angularly acquired projections over an 180^0 range. An ROI image in the phantom was selected to contain 80×80 pixels, which occupies only 8% of the global area. The truncated projection data were corrupted by Poisson noise to mimic real experimental conditions. The algebraic

This work was supported in part by the NSF-EEC#1238021.

reconstruction technique (ART) with total variation (TV) regularization was implemented to reconstruct the ROI image from the truncated projection data. The reconstruction method uses the reweighted L1 norm TV minimization, which allows a better approximation of the L0-norm than the L1-norm. While larger coefficients are penalized more in the L1-norm, the reweighted L1-norm enjoys a relatively uniform penalty for nonzero coefficients. Hence, the reweighted L1 norm may perform more effectively than the L1-norm for few-view reconstruction. Mathematically, we have

$$\begin{cases} \min\limits_{\mu} \sum\limits_{(i,j)\in ROI} w_{i,j} \cdot TV\left[\mu(i,j)\right] \\ s.t. \quad \mathbf{A}\cdot\mu = b \end{cases}, \tag{3}$$

where the reweighting factor is defined as $w_{i,j} = 1/(TV\left[\mu(i,j)\right]+\varepsilon)$, and ε is a parameter to avoid the singularity. Since the attenuation image is reconstructed via iteration, the reweighting factor is adaptively defined. Eq. (3) can be solved using the split-Bregman method. This method decomposes Eq. (3) into the L2 and L1 minimization steps. The conjugate gradient (CG) method will be used to solve the L2 minimization. The shrinkage operator will handle the L1 minimization. The split Bregman iteration should converge very quickly. The reconstructed image has a good contrast resolution, and the detailed features in the ROI are quantitatively accurate.

III. Results

A. Low Field Halbach MRI with Stationary CT Scanner

Fig. 1 shows the first design, which consists of a Low Field MRI that is generated using a Halbach array of 32 NdFeB magnets that are arranged to cancel out the fringe field on the outside. NdFeB generate homogenous fields, which makes them good candidates for MRI machines and are have been used in portable MRI machines have been for imaging plants and trees at ~0.1T strengths [12-14]. The arrays of 32 NdFeB magnets that are approximately 5 cm x 5cm x 5 cm

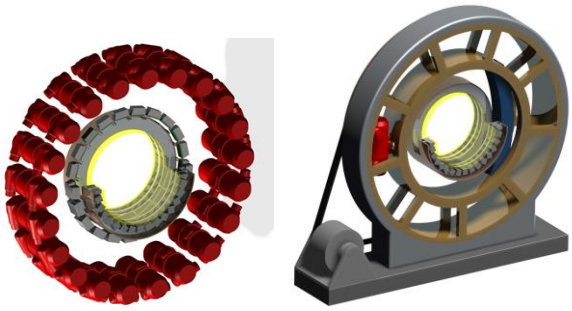

Fig. 1 Low Field MRI with Halbach array permanent magnets and stationary CT. (*Left*) Rendering of the 21 x-ray sources on the outside, with the detectors following in a separation of the Halbach aluminum rings at the center. Inside, 32 magnets are arranged with periodic directionality magnetic fields. (*Right*) With a minimal magnetic field, a standard rotating CT source can be implemented.

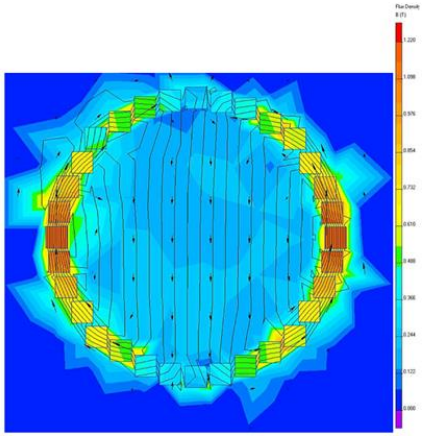

Fig. 2. A 2D magnetic field analysis in QuickField showing a uniform *0.2T field at the center and a 3mT field 55cm from the center. The physical properties of the magnets were altered to add directionality; ie, each magnetic field points in a different direction in the arrangement based on its location.*

in size are housed in aluminum, which is minimally magnetic. These 32 magnets make up one "ring", and additional rings stabilize the magnetic field at the center, while generating a larger FOV for imaging purposes.

Fig. 2 shows the 2D simulation of the magnetic field in QuickField. The center magnetic field was 0.20 T while at 55cm away from the midpoint, it dropped to 3 mT– which was the limit at which x-ray beam deflection and defocusing occurred as described. At 1m from the isocenter of the magnet, the magnetic field is a mere 7.5 * 10^{-5} T. The geometry was not exactly constant due to a few geometric defects, yet the field remains contained within the bore region. Instead of physically turning the magnets as shown in Fig. 1, the properties of the magnet were altered to have a directionality; ie, a magnet in the north least location, had its magnetic field aligned 45 degrees in a direction instead of physically turning the magnet. The physical properties (such as magnetization in a magnetic field) of the magnets were obtained using the B-H curve found from manufacturers online, and the aluminum is reported to have negligible magnetization potential and a relative permeability of 1.

The four rings of aluminum are thus arranged to have a total length of approximately 30 cm, with a gap at the center to allow the x-ray beam to travel through. The CT is located at this central location with a 1m gap from the center to the x-ray tubes, and consists of 21 source-detectors. The detector area is 100mm*100mm, SDD = 1175 mm, SOD = 750 mm, FOV = 64 mm. The gap is enlarged to 100 mm. As mentioned earlier, the CT will not be heavily affected by the fringe field. Furthermore, recent methods have shown that image reconstruction is possible with this FOV, and valuable information about the lung can be learned. The combination of MRI and CT simultaneously given this FOV can reveal the structural and functional physiology that may be absent with only one technique.

B. Solenoid Coils MRI with Stationary CT

Permanent magnets are a viable source for the magnetic field, but superconducting wires are much more commonly used in generating magnetic fields in MRI and are much more commercially available. Common high field MRI machines generate a main field up to 3T clinically, and the fringe fields are extremely large. Previous studies in trying to merge CT-MRI involved placing an x-ray source in a high field setting, or close to it, causing deterioration of the CT image quality. The 3D rendering is shown in Fig. 3, with the coiled rings surrounding the central bore as in a typical MRI. Since the magnetic field is only $6.42*10^{-4}$ T at the 1m mark, a CT scan can be placed with no detrimental effects. The component that is perpendicular to the anode is $3.5 *10^{-5}$ T, a field not strong enough to overcome the ~120 kV potential that directs the electron beam motion to the cathode.

By reducing the current and turns from the standard MRI solenoid setup, a weaker magnetic field can be generated. Using dimensions based on commercially available MRI magnets, a simulation was run with the current lowered as shown in Fig. 3. The "shorter" diameter coils represent the inner coils which generate the main magnetic field, while the outer diameter coils create an opposing magnetic field. This opposing magnetic field can greatly reduce the fringe field while maintaining a homogenous magnetic field at the center, and acts as an active shielding element described in previous papers. Running this rendition in Vizimag, an 82mT field is possible at the center and a 0.642 mT field at the 1m mark, where the CT scanner would be placed.

In terms of design, the inner diameter coils have current flow in one direction, while the current in the outer loops is in an opposite direction to create an active shielding mechanism that cancels out the fringe field at 1m. For dimensions, the inner diameter coils have 400 turns at 100 Amps and a diameter of 0.64m and a width of 0.1m. A 0.64m diameter was chosen since gradient coils need to be placed first, and they take up a small place and MRI systems generally have a 0.6m diameter. For the outer shielding coils, the diameter was changed to 1.2m. The thicker coils for the inner diameter pairing on the ends have a width of 0.2m. The x-axis placement of the coils were symmetric and centered at 0.1m, 0.2m, 0.3m, 0.8m, and 1m.

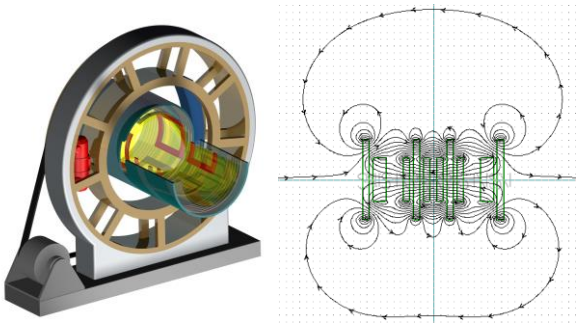

Fig. 3. **Solenoid MRI-CT**. *(Left) Coils are used on the inside to generate a stable magnetic field, with outer set of coils for active shielding. (Right) The solenoids were designed in Vizimag and it was shown that the B field could be concentrated at the center at ~82mT and decay to ~1.2mT 1m away from the center*

At this point, we note that the previous stationary CT can be replaced by a rotating CT scanner due to the small magnetic fields. Stationary CT were used to minimize any disturbances arising from the Lorentz force, but a standard rotating x-ray source can also be used. In addition, recent advances have stated that active and passive shielding inside the x-ray tubes can make rotating x-ray sources possible in weak magnetic fields. A lot of progress in this direction has been made thanks to groups working on Hybrid Linac-MRI machines [15, 16] for reducing interference between MRI and high energy x-ray systems.

C. Rotating Compact MRI-CT

The final design is based off developments in compact MRI that are portable yet have a sufficient magnetic field. In particular, compact MRI has been clinically used to image the brain intraoperatively, with sufficient gap to fit the patient's head. By targeting the lungs instead, it should be feasible to generate a similar magnetic field while making the gap between the permanent magnets a bit larger for chest imaging. Fig. 4 demonstrates the concept of using a compact MRI and integrating a CT within the perpendicular gap. C-arm CT systems are already available that have a similar design, so the combination of a compact MRI and a C-arm CT concept is shown with the two systems rotating around the patient as images are acquired.

In the rotating MRI-CT configuration, a CT scan is attached perpendicularly to the compact MRI system. C-arm CT scans are readily available, so this can be positioned in the same plane as the MRI, but in a perpendicular arrangement. This configuration allows both systems to rotate and acquire images simultaneously and reconstruction can be used to link both modalities. In this setup, the detector has to be placed on the inner surface of the arm connecting the permanent magnets. This placement is mandatory since the

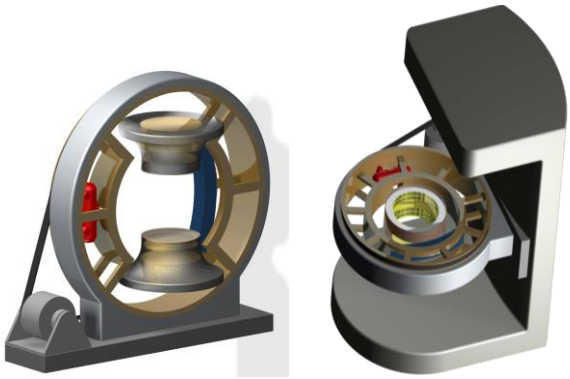

Fig. 4. **Rotating CT/MRI**. (*Left*) *Compact low field MRI with permanent magnets with a rotating gantry located perpendicularly. (Right) Design for vertical imaging*

magnetic field will be stronger in the attaching metal that connects the two magnets, allowing the x-ray source to occur at the open end and be free from magnetic effects.
It is desirable to image the patient in both supine and vertical positions, to measure the effects of gravity on lung function. Therefore, we have designed a vertical positioning system shown in Fig. 4, which can allow the patient to walk in and move down once the patient is positioned appropriately.

IV. Discussion & Conclusion

There have been few attempts to merge CT and MRI together due to the inherent physical conflicts between each component's needs. Attempts have been made to combine them, although not in a truly hybrid system, or one in a low field MRI. A more frequent method being employed is the use of a suite that has one section dedicated to CT and one dedicated to MRI, with an operating suite at the center. This allows the patient to be transported within the same suite between the three systems. While this may save time, it does not offer simultaneous acquisition. Furthermore, if the patient is attached to IV systems or has suffered a traumatic injury, it is disadvantageous to move the patient as it can be a threat to safety and the time needed to safely transport may be critical.

Interior tomography allows for a more compact system, such as the compact MRI and C-arm CT merge. The reconstruction of a sheep lung is shown in Fig. 5, which shows the reconstructed image was in an excellent agreement with the truth inside the ROI and is quantitatively accurate. Portable systems are highly favorable for intraoperative regions or quick diagnosis. Recent advances in scout-assisted interior tomography have shown that the time needed to obtain important information can also be improved. Advances in robust x-ray tubes within magnetic fields [5], effective combinations of hybrid linac machines, Halbach arrays [17] will propel the hybrid MRI-CT.

The combination of CT-MRI is a disruptive technology. The introduction of PET-CT and MRI-PET has dramatically changed the way physicians are able to access data for diagnosis and treatment in oncology, surgical planning, radiotherapy, etc. By introducing a CT-MRI system, the physician will be able to assess both the structure and functionality of organs simultaneously in a cost-effective and synergistic method. For a specific example, lung cancer can be imaged with CT revealing the air-tissue interfaces, nodules, tumors, and microstructures. MRI can measure airway functions described earlier to reveal the lung physiology. By combining these two, malignancy can be measured without biopsy or need to integrate two separately taken images. Currently, this concept relies on hyperpolarized gas. However, advances in ultra-low field MRI and image reconstruction techniques at low resolution would be applied to cover more regions in the future.

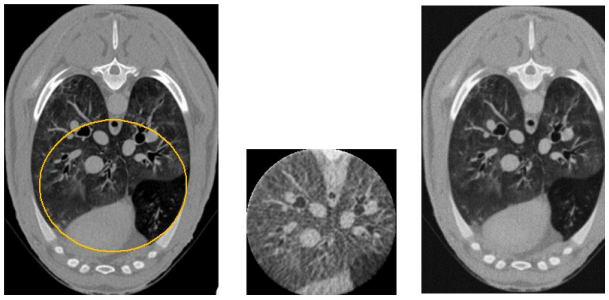

***Fig. 5. Interior reconstruction of a sheep lung numerical phantom**. (a) The ROI on original image. (b) Reconstructed ROI image using the 21 stationary source CS-based interior tomography algorithm. (c) Global reconstructed image using the CS-based reconstruction algorithm.*

References

[1] Hopkins, Susan Advances in magnetic resonance imaging of lung physiology. *J Appl Physiol* , 2007; 102: 1244-1254.

[2] Wen Z, Fahrig R, Conolly S, Pelc NJ. Investigation of electron trajectories of an x-ray tube in magnetic fields of MR scanners. *Med Phys,* 2007; 34: 2048-59.

[3] Wen Z, Fahrig R, Pelc NJ. Robust x-ray tubes for use within magnetic fields of MR scanners. *Med Phys,* 2005; 32: 2327-36.

[4] Brzozowski et all. Compatibility of interventional x-ray and magnetic resonance imaging: Feasibility of a closed bore XMR (CBXMR) system. *Med Phys,* 2006; 33: 3033-45.

[5] Lillaney P Fahrig R et al. Novel motor design for rotating anode x-ray tubes operating in the fringe field of a magnetic resonance imaging system. *Med Phys,* 2013; 40: 022302. doi: 10.1118/1.4773313

[6] Tsai L et al. An open-access, very-low-field MRI system or posture-dependent 3He human lung imaging. *Journal of Magnetic Resonance,* 2008; 193: 274-285.

[7] Yu HY, Wang G Compressed sensing based Interior tomography. *Phys Med Biol,* 2009 54: 2791–2805.

[8] Ye YB, Yu HY, Wei YC, Wang G. A general local reconstruction approach based on a truncated Hilbert transform. International Journal of Biomedical Imaging 2007: 63634.

[9] Yu HY, Yang JS, Jiang M, Wang G. Supplemental analysis on compressed sensing based interior tomography. Phys Med Biol, 2009; 54: N425–N432.

[10] Yu HY, Ye YB, Wang G. Local Reconstruction Using the Truncated Hilbert Transform via Singular Value Decomposition. Journal of X-Ray Science and Technology, 2008; 16: 243–251.

[11] Wang G, Zhang J, Gao H, Weir V, Yu H, et al. Towards Omni-Tomography—Grand Fusion of Multiple Modalities for Simultaneous Interior Tomography. PLoS ONE, 2012; 7(6): e39700. doi:10.1371/journal.pone.0039700

[12] Jones M. A transportable magnetic resonance imaging system for in situ measurements of living trees: The Tree Hugger. Journal of Magnetic Resonance, 2012; 218: 133-140.

[13] Windt C, Soltner H, Dusschoten D, Blumler P. A portable Halbach magnet that can be opened and closed without force: The NMR-CUFF. Journal of Magnetic Resonance, 2011; Vol 208(1): 27-33.

[14] Wroblewsi P, Mandhala Magnet for Ultra Low-Field MRI. IEEE, 2011; Doi: 1109/IST.2011.5962203

[15] Aubin J, Fallone B. Mangetic decouping of the linac in a low field biplanar linac-MRI. *Med Phys*, 2010; 37(9): 4755-61.

[16] Tadic T. Design and Optimization of a Novel Bored Biplanar Permanent-Magnet Assembly for Hybrid Magnetic Resonance Imaging Systems. *IEEE Transactions on Magnetics*, 2010; Vol 46, 12.

[17] Raich H. Design and Construction of a Dipolar Halbach Array with a Homogenous Field from Identical Bar Magnets: NMR Mandhalas. *Concepts in Magnetic Resonance Part B*, 2004; Vol. 23B(1) 16–25